

ParticleGS: Learning Neural Gaussian Particle Dynamics from Videos for Prior-free Physical Motion Extrapolation

Jinsheng Quan¹, Qiaowei Miao¹, Yichao Xu¹, Zizhuo Lin¹, Ying Li², Wei Yang³, Zhihui Li⁴, Yawei Luo¹ 

¹Zhejiang University ²North China University of Technology

³Huazhong University of Science and Technology ⁴University of Science and Technology of China

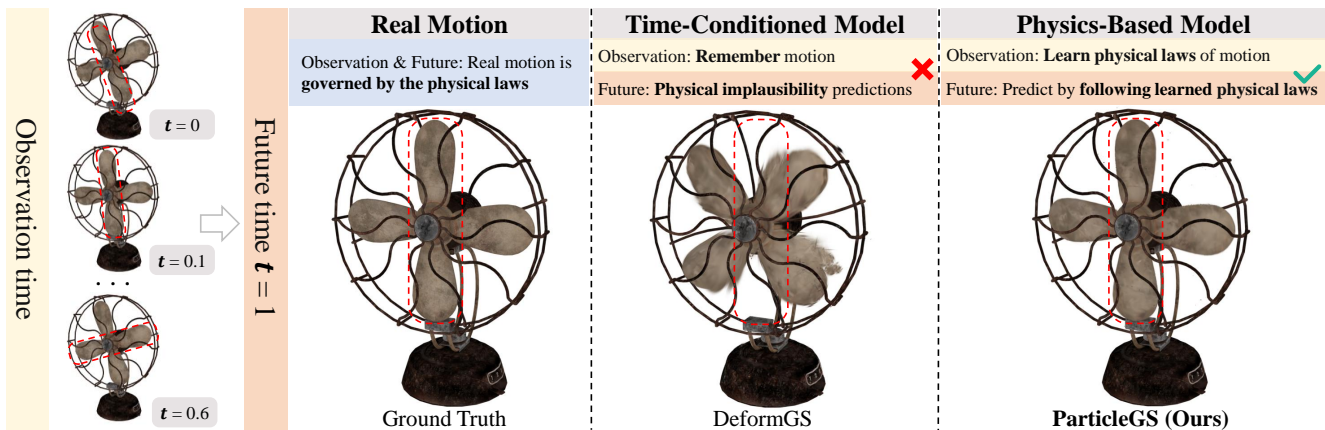


Figure 1. **Example of typical reconstruction method and our method for extrapolation.** Given multi-view RGB video observations, our **ParticleGS** can learn latent physical dynamics and use them to extrapolate future Gaussians with physically consistent motion and appearance. In contrast, existing time-conditioned deformation methods fail to predict plausible future motion.

Abstract

The ability to extrapolate dynamic 3D scenes beyond the observed timeframe is fundamental to advancing physical world understanding and predictive modeling. Existing dynamic 3D reconstruction methods have achieved high-fidelity rendering of temporal interpolation, but typically lack physical consistency in predicting the future. To overcome this issue, we propose **ParticleGS**, a physics-based framework that reformulates dynamic 3D scenes as physically grounded systems. **ParticleGS** comprises three key components: 1) an encoder that decomposes the scene into static properties and initial dynamic physical fields; 2) an evolver based on Neural Ordinary Differential Equations (Neural ODEs) that learns continuous-time dynamics for motion extrapolation; and 3) a decoder that reconstructs 3D Gaussians from evolved particle states for rendering. Through this design, **ParticleGS** integrates physical reasoning into dynamic 3D representations, enabling accurate and consistent prediction of the future. Experiments show that **ParticleGS** achieves state-of-the-art performance in extrapolation while maintaining rendering quality comparable to leading dynamic 3D reconstruction methods.

1. Introduction

Learning the physical dynamics from multi-view videos and inferring the subsequent motion is crucial for applications like gaming, autonomous driving, and robotics [53, 60]. Recent methods [3, 12, 38, 43, 54, 58, 59] have demonstrated impressive results in reconstructing and rendering vivid dynamic 3D scenes. Nevertheless, these methods typically predict deformation as a function of time. While this formulation suffices for interpolating motion within the observed temporal range, it fails to learn the underlying physical laws. This results in unsatisfactory performance when extrapolating to unseen future states, as shown in Fig. 1.

To overcome these limitations, incorporating physical laws into dynamic 3D scene modeling has emerged as a promising direction [4, 9, 15, 50]. Existing approaches can be broadly categorized into two types. The first explicitly injects **physics priors** through simulation frameworks [13, 16, 33, 56], physics-informed neural networks [7, 8, 25, 45], or architectures with built-in physical constraints [25, 61]. While enhancing physical plausibility, such methods often depend on manually specified external forces or restrictive assumptions, limiting their flexibility and generalization.

The second line of work inherently relies on **geometric priors**, such as pre-processed point clouds or meshes, to infer physical information [20, 36, 41, 63]. However, these methods cannot directly capture dynamics from raw observations and typically require multi-stage optimization. More recent works have modeled Gaussian rigid motion using velocity and acceleration fields [26, 27]. Nevertheless, such low-order dynamics are insufficient to accurately capture complex deformations, making it still challenging to learn physical dynamics directly from raw observations.

In this paper, we propose ParticleGS, a dynamic 3D representation framework based on 3DGS [22] from the perspective of physical particle dynamics. Our key insight is to treat each Gaussian as a particle, whose temporal evolution is driven by **physical state vector** governed by the underlying physical laws. To this end, ParticleGS comprises three key components: 1) A Dynamics Latent Space Encoder that maps each Gaussian to an initial latent physical state vector, which is factorized into static properties (*e.g.*, mass, material) and initial time-varying dynamic properties (*e.g.*, velocity, acceleration). 2) A Neural ODE-based Dynamics Evolver, the core of our approach, which learns a continuous Markov state transition function in the latent space to approximate the underlying physical dynamics (*e.g.*, Newtonian or Navier–Stokes) governing the particles, rather than merely memorizing temporal deformations. 3) A Gaussian Space Decoder that translates the evolved latent states back into the deformation of each Gaussian for rendering. By focusing on learning the underlying dynamics rather than memorizing temporal deformation, ParticleGS achieves extrapolation beyond observations.

Our neural dynamics modeling distinguishes ParticleGS from existing approaches. Compared with time-conditioned reconstruction methods [54, 58, 59], ParticleGS learns neural dynamics directly from videos, enabling physically consistent extrapolation beyond observed frames. Unlike methods that rely on physical or geometric priors [25, 56], it requires no predefined physical laws or structured geometric inputs, achieving prior-free dynamic learning. In contrast to approaches that model specific low-order physical quantities, such as velocity fields [26, 27], ParticleGS learns a generalized formulation of higher-order particle dynamics through neural ordinary differential equations. The main contributions are summarized as follows:

- From a physical perspective, we reformulate time-conditioned deformation using neural ordinary differential equations, enabling a physics-grounded representation of the driving dynamics.
- We propose ParticleGS, an Encoder–Evolver–Decoder framework that represents the scene as a physical particle system with static properties and initial dynamic fields, where a Neural ODE-based evolver learns and extrapolates the latent physical laws directly from observations.

- Numerical experiments show that our method achieves the best performance in future Gaussian extrapolation on multiple datasets.

2. Related Work

Time-Conditioned Dynamic 3D Reconstruction. Novel view synthesis for dynamic scenes has been significantly advanced by Neural Radiance Fields (NeRF) [39] and 3D Gaussian Splatting (3DGS) [22]. To model temporal variations, a common strategy is to learn a deformation field that maps a canonical representation to the scene’s state at any given time [42, 43, 59]. For NeRF-based methods, significant research has focused on improving representation efficiency and quality. This includes decomposing the 4D spacetime into lower-dimensional components like planes [3, 14, 49] and employing compact yet expressive features such as hash encodings [12, 40]. Following a similar trajectory, dynamic 3DGS methods [1, 18, 21, 23, 32, 35, 37, 52, 55] extend static Gaussian clouds with learned motion, enabling high-fidelity, real-time rendering.

Injecting Physical Priors into Dynamic 3D. To endow 3D representations with predictive power, integrating physical principles is a promising direction. One line of work follows the Physics-Informed Neural Network (PINN) paradigm [45], embedding governing equations like the Navier–Stokes equations directly into the learning objective to constrain motion [7, 17, 19, 25]. While effective, this approach is often confined to systems with well-defined physical laws and may not generalize to complex scenes. Another strategy involves integrating differentiable physics simulators [10, 11, 29, 30], which provide strong physical priors. In addition, some methods embed rigid-body constraints, springs, or incorporate Graph Neural Networks [34] to embed neighborhood constraints [5, 47, 61, 62].

Learning Physical Information from Vision. Inferring physical laws and properties directly from visual observations has attracted increasing interest. One line of work focuses on recovering object-level physical attributes, such as material properties [2, 13, 28, 33], physically plausible geometry [16, 57], and velocity fields for motion extrapolation [26, 27]. Another line aims to learn underlying physical equations, including neural constitutive models [36] and neural dynamics equations [4, 15, 31]. However, existing Neural ODE-based methods [20, 36, 41] struggle to learn particle-level dynamics purely from RGB videos.

Neural Ordinary Differential Equations. Unlike traditional discrete-layer architectures, Neural ODEs [6] integrate continuous-time dynamical systems with neural networks. Specifically, they use a neural network f to learn the derivative of the system’s state. By employing an adaptive ODE solver to integrate this learned function over time, these models enable the learning of state evolution. This makes them well-suited for modeling physical processes.

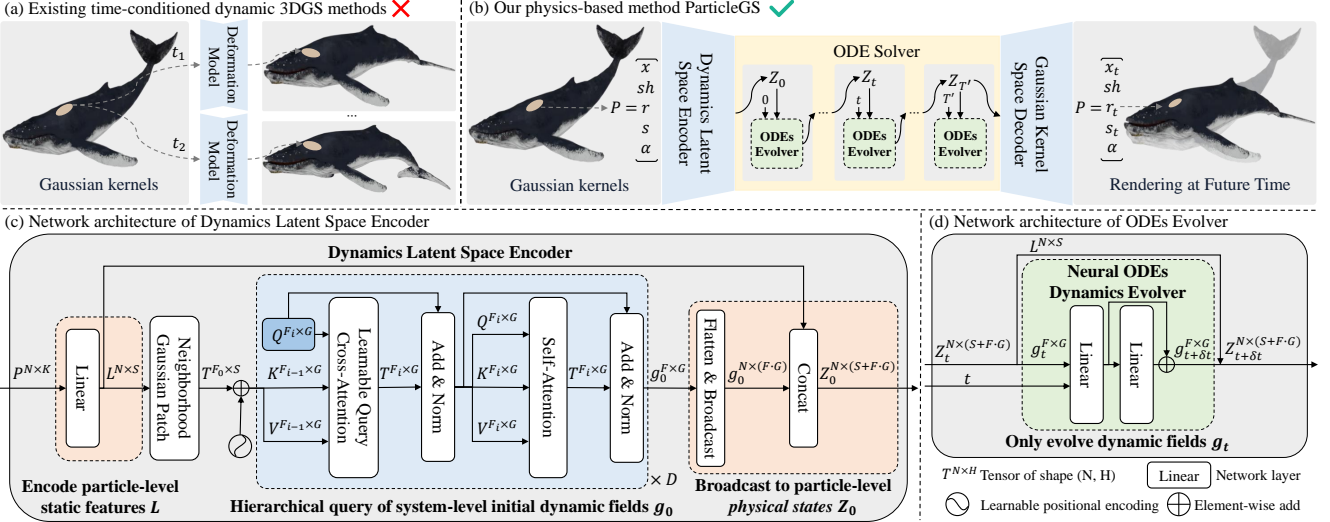


Figure 2. **Overview of ParticleGS.** (a) Existing time-conditioned methods learn a deformation model for each independent discrete time. (b) Our physics-based framework, ParticleGS, uses latent physical states to drive 3D Gaussian deformation, enabling motion extrapolation. (c) The Dynamics Latent Space Encoder maps Gaussians to an initial physical state, factorized into static properties and dynamic fields. (d) The Neural ODEs Evolver learns the underlying physical laws by modeling the continuous-time evolution of the dynamic fields.

3. Methodology

We begin by formulating the dynamic scene representation and positioning our physics-based approach against existing methods in Sec. 3.1. We then detail the architecture of our framework, ParticleGS, in Sec. 3.2 and describe its optimization strategy in Sec. 3.3.

3.1. Problem Formulation and Overview

3D Gaussian Splatting for Static Scenes. 3D Gaussian Splatting [22] aims to learn a set of Gaussian kernels $P = \{p_i\}_{i=1}^N$ from a set of images taken from corresponding camera viewpoints. Given a differentiable renderer \mathcal{R} and a viewpoint v , an image \hat{I}^v is rendered as:

$$\mathcal{R}(P, v) = \hat{I}^v. \quad (1)$$

Here, each Gaussian kernel p is defined by a set of optimizable parameters $\{x, sh, r, s, \alpha\}$, with x as position, sh as Spherical Harmonics coefficients, r as rotation, s as scaling, and α as opacity. The Gaussian set is typically initialized from an SfM reconstruction [48] or a random point cloud.

Time-Conditioned Dynamic Scene Representation. To model dynamic scenes, existing methods extend the static 3DGS framework. For a set of videos captured from corresponding viewpoints over T discrete time steps, the primary goal is to learn a representation that can render the scene. These methods [54, 58, 59] typically learn a canonical set of 3D Gaussians P and a time-conditioned deformation model $\mathcal{D}(P, t) = P_t$, which deforms P into the Gaussian set P_t at time t , as shown in Fig. 2(a). The image at time $t \in [0, T]$ and a viewpoint v is rendered by:

$$\mathcal{R}(\mathcal{D}(P, t), v) = \hat{I}_t^v. \quad (2)$$

However, these methods lack the modeling of underlying physical laws, which limits their ability to extrapolate. To address this, we propose to model the dynamic 3D scene as a system of particles governed by neural physical dynamics.

Physical Dynamics-Based Representation (Ours). For the same input, we employ the physical state set Z_t to drive the Gaussian particles at time t . Under this definition, an image at time $t \in [0, T']$ (where T' may extend beyond the observed time T) and a viewpoint v is rendered as:

$$\mathcal{R}(D(P, Z_t), v) = \hat{I}_t^v. \quad (3)$$

Here, D is a decoder that deforms the canonical Gaussians. The state set Z_t is evolved from an initial state Z_0 , which is encoded from the canonical Gaussians P .

Comparing Eq. 3 with Eq. 2, our method drives the 3D Gaussians by the physical state rather than merely the timestamp t . This brings advantages: 1) Spatiotemporal awareness: Z_t implicitly encodes the entire system history from 0 to t , while t encodes temporal order only; 2) Physical plausibility: Conditioning on a state Z_t is more consistent with physical particle systems; 3) Markov property: The evolution from Z_t is Markovian, as Z_t contains all necessary information to predict the next state. Time-conditioned models lack this, as timestamps t_1 and t_2 are independent.

The framework of ParticleGS is shown in Fig. 2(b). ParticleGS consists of three components: 1) a Dynamics Latent Space Encoder that maps Gaussians P to their initial physical states Z_0 ; 2) a Neural ODE-based Dynamics Evolver that models continuous dynamics to evolve Z_0 to Z_t using a Neural ODE solver; and 3) a Gaussian Kernel Space Decoder that maps the evolved physical states Z_t to the deformation of canonical Gaussian P to form P_t for rendering.

3.2. ParticleGS

Dynamics Latent Space Encoder. Unlike existing methods that encode each Gaussian independently, we propose a Dynamics Latent Space Encoder to reduce the evolution complexity of the physical states via shared dynamic fields.

For a scene containing N Gaussians, if the state of each Gaussian is represented by a G -dimensional vector, directly evolving all $N \times G$ parameters independently is computationally prohibitive for large N . We observe that in physical particle systems such as the Material Point Method [51], each particle retains static properties (e.g., mass, material), while its temporal evolution is driven by **shared** dynamic fields (e.g., gravitational fields) across particles.

Following this idea, we factorize the state of the Gaussians into two components: 1) a set of N particle-level static features $L \in \mathbb{R}^{N \times S}$, and 2) a set of F system-level dynamic fields $g_t \in \mathbb{R}^{F \times G}$ that are shared across all Gaussians. The **physical state** set Z_t for all Gaussians is defined as:

$$Z_t = \text{concat}[L, \mathbf{1}_N \otimes g_t^{\text{flat}}], \quad Z_t \in \mathbb{R}^{N \times (S+F \cdot G)}. \quad (4)$$

Here, $g_t^{\text{flat}} \in \mathbb{R}^{1 \times (F \cdot G)}$ is the flattened dynamic fields, $\mathbf{1}_N \in \mathbb{R}^{N \times 1}$ is a vector of ones, and the Kronecker product $\mathbf{1}_N \otimes g_t^{\text{flat}}$ broadcasts the global field to all N particles. By evolving only F dynamic fields rather than all N particle states, we reduce the computational complexity of the dynamics evolver from $\mathcal{O}(NG)$ to $\mathcal{O}(FG)$, where $F \ll N$.

To obtain the initial physical state Z_0 , we design a Dynamics Latent Space Encoder f_{encoder} as shown in Fig. 2(c). Gaussian features are first transformed into static features L via linear layers. To handle different numbers of Gaussian particles, neighborhood Gaussian patches are constructed by farthest point sampling and k -nearest neighbors within a Mini-PointNet++ module [44]. Finally, we employ cross-attention blocks with F learnable queries and self-attention to hierarchically aggregate F initial dynamic fields g_0 . Thus, the initial physical state set for the Gaussians Z_0 is encoded by f_{encoder} according to Eq. 4 as:

$$f_{\text{encoder}}(P) = Z_0. \quad (5)$$

Here P is the canonical Gaussian set, and each $p \in P$ is a Gaussian kernel with its parameters $\{x, sh, r, s, \alpha\}$.

The F dynamic fields can be interpreted as a basis decomposition of the dynamics, where each field captures a distinct motion mode. To further analyze the role of physical states, we visualize them in RGB as shown in Fig. 3. It shows that: 1) Dynamic Coherence: The physical states Z_t are not arbitrary but are strongly correlated with the motion patterns of the scene; 2) Temporal Stability: These stable and smooth physical states reflect a continuous and consistent physical evolution learned by the model.

Neural ODEs Dynamics Evolver. Once the 3D Gaussians are encoded into the initial physical states, the core

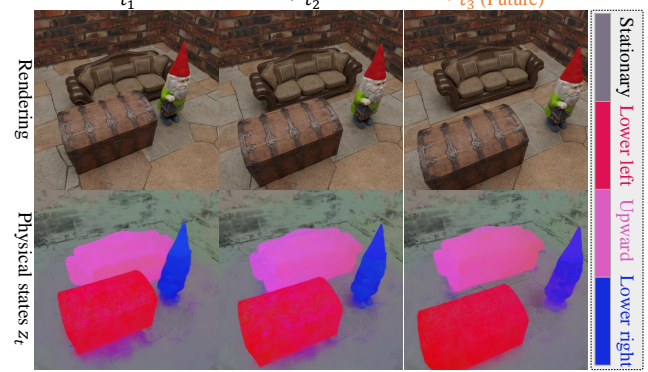


Figure 3. Rendering and visualization of physical states. Motion-similar Gaussians exhibit comparable features, and their physical states change stably over time.

problem becomes evolving this state in a physically plausible manner. Rather than relying on low-order dynamics methods such as a velocity field, we propose a Neural ODEs Dynamics Evolver that models higher-order dynamics.

Although the factorized encoding balances efficiency and representational capacity, a key challenge remains: in real motion, physical fields are often governed by high-order differential equations (e.g., Newton's laws). Discrete-step models such as RNNs or MLPs, which model discrete updates, may struggle to capture continuous-time, high-order dynamics without careful design [6].

To model such dynamics, we recall that any n -th order differential equation

$$\frac{d^n x}{dt^n} = f\left(x, \frac{dx}{dt}, \dots, \frac{d^{n-1}x}{dt^{n-1}}, t\right) \quad (6)$$

can be equivalently written as a *first-order* system F by augmenting the state with its successive derivatives:

$$X = \left(x, \frac{dx}{dt}, \dots, \frac{d^{n-1}x}{dt^{n-1}}\right), \quad \frac{dX}{dt} = F(X, t). \quad (7)$$

This formulation shows that a first-order system defined on an augmented latent space is expressive enough to represent any high-order dynamics.

Based on this principle, we use our dynamic fields g_t to represent this augmented state and use a Neural ODE-based network f_{evolver} to model the high-order dynamics as visualized in Fig. 2(d):

$$\frac{dg_t}{dt} = f_{\text{evolver}}(g_t, t). \quad (8)$$

The dynamic fields at any future time $t + \delta t$ are then obtained by integrating f_{evolver} using a numerical ODE solver:

$$\begin{aligned} g_{t+\delta t} &= g_t + \int_t^{t+\delta t} f_{\text{evolver}}(g_\tau, \tau) d\tau \\ &= \text{ODESolver}(f_{\text{evolver}}, g_t, t, t + \delta t). \end{aligned} \quad (9)$$

Here, we use the common Runge–Kutta (RK4) [24] method as the numerical ODE solver.

Instead of memorizing a trajectory, our f_{evolver} learns to model the local high-order derivatives governing the dynamic fields. As a result, the learned physical laws can be explicitly followed by integrating f_{evolver} , enabling stable and physically consistent extrapolation.

Gaussian Kernel Space Decoder. Following existing methods [26], we decompose each Gaussian kernel’s motion into translation and rotation by Rodrigues’ rotation formula [46]. Specifically, the decoder predicts a translation vector T , a motion rotation vector R , and deformation terms $\{\delta r, \delta s\}$, which are used to update the parameters of Gaussian kernels $\{x, r, s\}$ as:

$$x_t = x + \text{Rod}(R)x + T, \quad r_t = r \circ \delta r, \quad s_t = s + \delta s. \quad (10)$$

Here $\text{Rod}(R)$ is the rotation matrix generated from R via Rodrigues’ formula [46], and \circ is the quaternion product.

We implement the decoder using a multi-head MLP f_{decoder} , which maps each particle’s physical state $z_t \in Z_t$ to its corresponding deformation parameters:

$$f_{\text{decoder}}(z_t) = \{T, R, \delta r, \delta s\}. \quad (11)$$

The final Gaussian parameters p_t are obtained by applying these deformations to the original parameters p by Eq. 10.

This motion factorization enables the model to learn meaningful physical components of motion.

3.3. Optimization

Following [59], we jointly optimize the Gaussian kernels and the ParticleGS network using \mathcal{L}_1 loss and D-SSIM loss:

$$\mathcal{L} = \mathcal{L}_1 + \mathcal{L}_{D-SSIM}. \quad (12)$$

Progressive Training. Directly optimizing both geometry and the Neural ODE-based deformation model from video supervision can lead to unstable training, as the ODE solver may propagate errors in early steps. To mitigate this, we adopt a progressive training schedule that gradually introduces complexity: 1) Geometry warm-up: freeze ParticleGS and optimize the Gaussian kernels at $t = 0$; 2) Dynamics warm-up: freeze the Gaussian kernels and gradually expand the temporal window, allowing ParticleGS to learn deformation trends; 3) Joint optimization: optimize both the Gaussian kernels and ParticleGS.

Dynamic Gaussian Optimization. Following standard 3DGs [22] and the existing dynamic 3DGs methods [27, 54, 59], we periodically apply densification and pruning, meaning the total Gaussian count N changes during training. For static feature L , the Encoder and Decoder MLPs treat the N particles as a batch, operating on each independently as in existing methods. For initial dynamic fields g_0 , we use a Mini-PointNet++ module to form

a fixed number of neighborhood patches and use the Cross-Attention module to aggregate F dynamic fields, thus it maps a variable-sized input N to a fixed-size output F .

Neighborhood Regularization. To ensure the encoder is robust to different local particle structures resulting from densification, we propose an online neighborhood regularization. Instead of computing the neighborhood graph using Mini-PointNet++ only once, we periodically regenerate the neighborhood patches during training. This acts as a data augmentation, enhancing the robustness of the encoder for extracting the initial dynamic fields g_0 .

See Appendix for more implementation details.

4. Experiments

4.1. Experimental Setup

Datasets. This work’s primary focus is **temporal motion extrapolation**, rather than only spatial novel view synthesis of observed frames. To this end, we follow the experimental setup of the most closely related works, NVFi [25] and FreeGave [27], and conduct our primary evaluations on the Dynamic Object Dataset and Dynamic Indoor Scene Dataset, which are specifically designed for extrapolation tasks [25]. Furthermore, we evaluate on Dynamic Multipart [26] and the challenging real-world dataset FreeGave-GoPro [27]. A brief description of the datasets is as follows: 1) *Dynamic Object Dataset*: Contains 6 objects exhibiting a wide range of motions, including complex non-linear motions of deformable animals such as flying and swimming; 2) *Dynamic Indoor Scene Dataset*: Consists of 4 scenes with multiple objects undergoing compositional motions; 3) *Dynamic Multipart*: Includes four objects with distinct multi-part motions. 4) *FreeGave-GoPro*: Covers 6 human interactions with objects in the real world. Following [25, 27], all datasets are divided into subsets for *reconstruction* and *extrapolation* tasks by training on the first 75% of video frames and test on the remaining 25%.

Baselines. The key distinction of ParticleGS lies in its physics-based modeling and its ability to learn high-order dynamics by Neural ODEs. To evaluate the distinctions of ParticleGS over baselines, we select three categories of baselines: 1) Representative methods based on time-deformation modeling: HexPlane [3], TiNeuVox [12], DeformGS [59], and Grid4D [58] are representative reconstruction methods; 2) Methods that embed physical information for motion extrapolation: NVFi [25] is a PINN-based method that embeds the Navier-Stokes equations, GaussianPrediction [61] is a GCN-based method that embeds time-invariant rigid neighborhood relations; 3) State-of-the-art velocity field-based method for extrapolation: FreeGave [27] and TRACE [26] learn motion via divergence-free velocity fields. All methods are run on a single RTX 4090 with 24GB GPU memory, except for an ablation study run on an A6000 with 48GB.

Table 1. Quantitative results on the Dynamic Objects and Dynamic Indoor Scene dataset, rendered at the source resolution. **Bold** and underline indicate the best and second best performance.

Method	Dynamic Object Dataset (Synthetic)						Dynamic Indoor Scene Dataset (Synthetic)					
	Reconstruction			Extrapolation			Reconstruction			Extrapolation		
	PSNR↑	SSIM↑	LPIPS↓	PSNR↑	SSIM↑	LPIPS↓	PSNR↑	SSIM↑	LPIPS↓	PSNR↑	SSIM↑	LPIPS↓
HexPlane [3]	21.585	0.910	0.125	22.418	0.934	0.078	17.978	0.482	0.626	23.192	0.671	0.474
TiNeuVox [12]	20.278	0.927	0.104	19.513	0.935	0.080	<u>23.706</u>	<u>0.681</u>	<u>0.373</u>	21.111	0.714	0.333
DeformGS [59]	37.376	0.964	0.034	26.163	0.946	0.038	20.020	0.595	0.445	21.982	0.769	0.233
Grid4D [58]	37.583	0.961	0.034	27.674	0.949	0.080	20.548	0.590	0.442	20.633	0.736	0.284
NVFi [25]	29.390	0.969	0.047	26.821	0.968	0.047	17.117	0.494	0.669	23.716	0.672	0.502
GSPrediction [61]	36.408	0.978	0.033	23.154	0.932	0.081	16.154	0.585	0.600	20.017	0.689	0.343
TRACE [26]	38.006	<u>0.991</u>	<u>0.011</u>	33.356	<u>0.983</u>	<u>0.013</u>	22.846	0.642	0.377	<u>29.476</u>	0.849	<u>0.205</u>
FreeGave [27]	<u>38.637</u>	0.992	<u>0.011</u>	<u>33.632</u>	<u>0.983</u>	0.012	19.681	0.589	0.453	28.983	<u>0.854</u>	0.212
ParticleGS	39.782	0.992	0.009	36.471	0.984	0.012	25.504	0.748	0.291	31.103	0.892	0.133

Table 2. Quantitative results on the Dynamic Multipart dataset and FreeGave-GoPro dataset, rendered at the source resolution. **Bold** and underline indicate the best and second best performance.

Method	Dynamic Multipart Dataset (Synthetic)						FreeGave-GoPro Dataset (Real World)					
	Reconstruction			Extrapolation			Reconstruction			Extrapolation		
	PSNR↑	SSIM↑	LPIPS↓	PSNR↑	SSIM↑	LPIPS↓	PSNR↑	SSIM↑	LPIPS↓	PSNR↑	SSIM↑	LPIPS↓
DeformGS [59]	38.430	<u>0.988</u>	0.019	27.989	0.942	0.045	20.106	0.832	0.212	21.665	0.858	0.195
TRACE [26]	36.269	0.990	0.021	33.458	<u>0.984</u>	<u>0.015</u>	20.103	<u>0.838</u>	0.205	25.915	0.892	0.163
FreeGave [27]	36.142	0.990	<u>0.020</u>	<u>33.526</u>	0.981	0.019	19.953	<u>0.838</u>	<u>0.206</u>	<u>26.510</u>	0.896	<u>0.160</u>
ParticleGS	38.608	0.990	0.019	36.136	0.985	0.014	20.116	0.839	0.205	26.789	0.903	0.150

Table 3. Quantitative results of FPS↑. **Bold** and underline indicate the best and second best performance.

Method	Dynamic Object Dataset	Dynamic Indoor Scene Dataset
TRACE [26]	51.041	39.590
FreeGave [27]	32.303	32.129
ParticleGS	<u>44.293</u>	<u>37.109</u>

Metrics. We follow existing dynamic 3D extrapolation works [25–27] and use the standard **PSNR**, **SSIM**, **LPIPS**, and **FPS** metrics to evaluate the dynamic 3D reconstruction and future frame extrapolation tasks.

4.2. Comparisons with Prior Work

We first compare all the methods on the Dynamic Object Dataset and the Dynamic Indoor Scene Dataset. Then, we compare 3 representative methods on the Dynamic Multipart and the challenging GoPro Dataset.

Quantitative results of performance & Analysis. Tables 1 and 2 show that our method achieves the best performance in both reconstruction and extrapolation tasks.

On the extrapolation task, our method exhibits significant advantages: 1) Compared to existing time-conditioned methods and approaches that inject physical priors, our method achieves a substantial PSNR improvement of over 5 dB across all datasets. This result suggests that our model successfully learns the underlying physical laws from observational data and follows them during extrapolation. 2)

Furthermore, ParticleGS outperforms velocity field-based extrapolation methods, such as TRACE and FreeGave, by an average PSNR margin of nearly 2.5 dB on synthetic datasets. This performance advantage extends to the challenging real-world FreeGave-GoPro Dataset. This indicates that our method can capture complex high-order dynamics more accurately than such low-order velocity field-based methods, leading to superior predictive accuracy.

For the reconstruction task, our method also achieves the best performance across all datasets. This demonstrates that our modeling framework is superior to or comparable to existing reconstruction methods.

Quantitative results of speed & Analysis. Tab. 3 shows that our method achieves a rendering speed comparable to velocity field-based approaches. Although we incorporate Neural ODEs, our physical state formulation requires only a single forward evaluation of the F dynamic fields, rather than computing the velocity of all N Gaussians. This validates the efficiency of our physical state design.

Qualitative comparisons of visualization results. As shown in Fig. 4 and Fig. 5, our method demonstrates superior visual fidelity and physical consistency compared to existing approaches: 1) For the representative time-conditioned methods TiNeuVox and DeformGS, the predicted results highlighted by red boxes exhibit clear spatial misalignments, whereas our method accurately aligns with the ground-truth locations. This demonstrates that our ap-

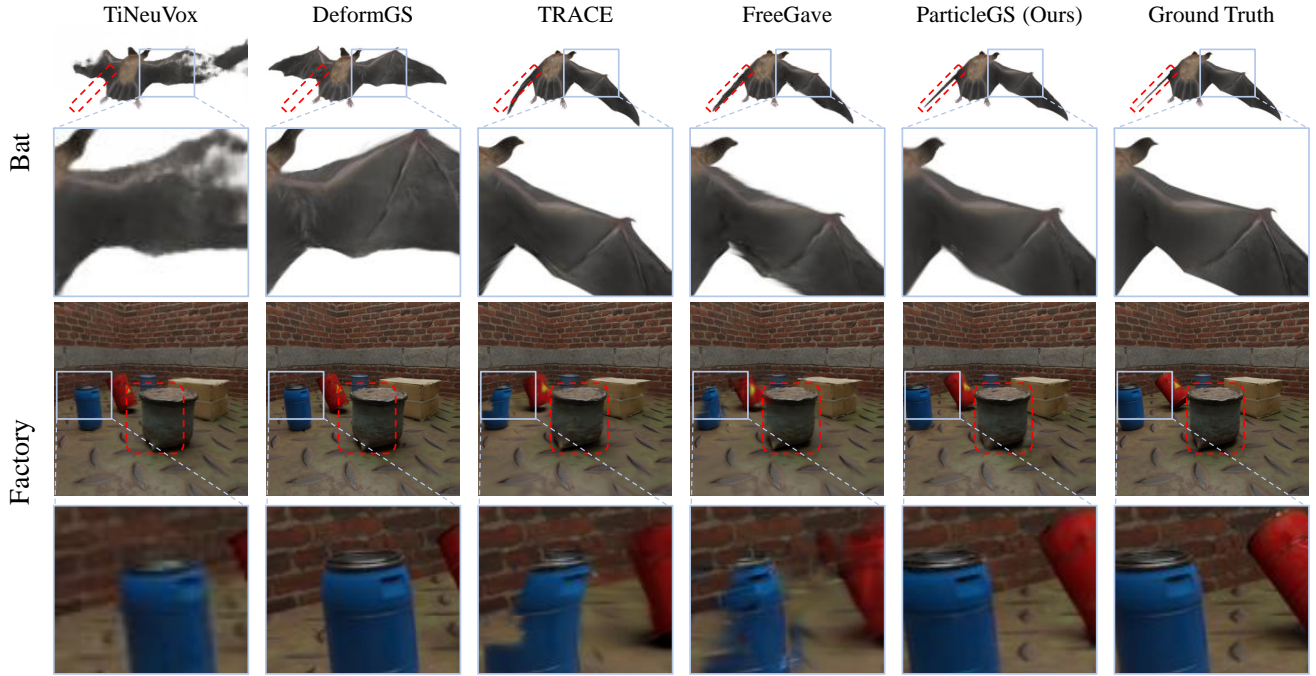


Figure 4. Qualitative results of extrapolation at a novel view and a future time on the Dynamic Object Dataset (Bat) and the Dynamic Indoor Scene Dataset (Factory). Red boxes indicate ground truth locations, and blue boxes highlight details.

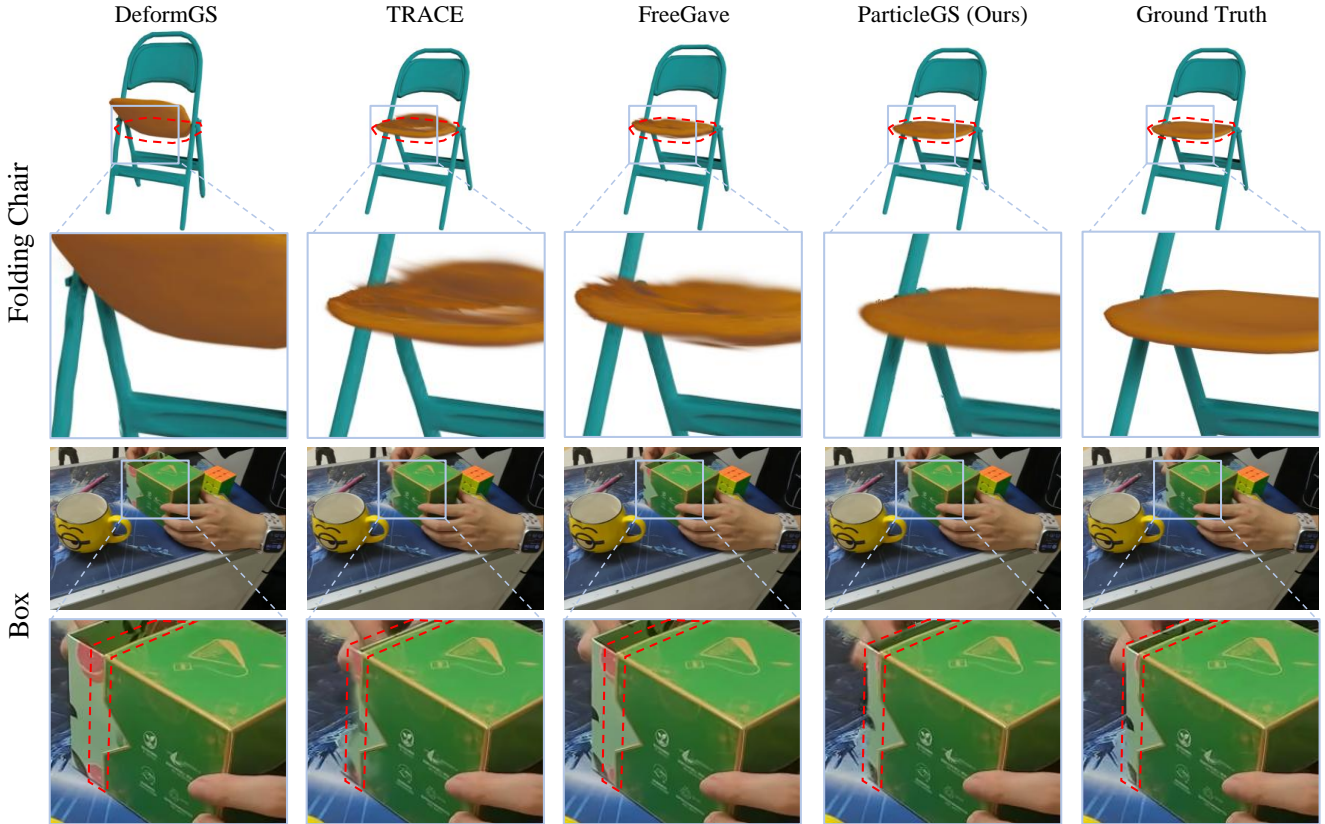


Figure 5. Qualitative results of extrapolation at a novel view and a future time on the Dynamic Multipart Dataset (Folding Chair) and the FreeGave-GoPro Dataset (Box). Red boxes indicate ground truth locations, and blue boxes highlight details.

Table 4. Results of extrapolation ablation studies. The method marked * indicates it is run on an A6000 with 48GB.

Method	Encoder	Evolver	Decoder	Optimize	F	Dynamic Object Dataset			Dynamic Indoor Scene Dataset		
						PSNR↑	SSIM↑	LPIPS↓	PSNR↑	SSIM↑	LPIPS↓
(1) *	w/o FE	full	full	full	x	36.391	0.982	0.012	-	-	-
(2.1)	full	full	full	full	1	35.206	0.982	0.012	28.026	0.883	0.174
(2.2)	full	full	full	full	4	36.236	<u>0.983</u>	0.012	30.977	<u>0.890</u>	<u>0.135</u>
(2.3)	full	full	full	full	16	36.552	0.984	0.012	<u>31.065</u>	0.892	0.133
(3)	full	w/o ODEs	full	full	8	34.551	0.981	0.015	27.455	0.861	0.179
(4)	full	full	w/o PD	full	8	35.343	0.982	0.014	28.653	0.879	0.198
(5)	full	full	full	w/o PT	8	35.438	0.979	0.015	29.168	0.883	0.218
(6)	full	full	full	w/o NR	8	35.986	0.981	0.015	30.232	<u>0.890</u>	0.161
ParticleGS	full	full	full	full	8	<u>36.471</u>	0.984	0.012	31.103	0.892	0.133

proach can extrapolate more physically consistent Gaussian deformations. 2) In the Factory and Folding Chair datasets, velocity field-based TRACE and FreeGave yield blurrier results than ParticleGS, and in the Box real-world dataset, their motion predictions appear noticeably misaligned. In contrast, ParticleGS delivers clearer and more physically plausible results, validating the effectiveness of our high-order dynamic modeling enabled by Neural ODEs.

4.3. Ablation Studies and Analysis

To investigate the impact of different components of our framework, we conducted the following ablation studies.

(1) Effect of Factorized Encoding (FE) in Eq. 4. Instead of decomposing the latent state into static properties l and dynamic fields g_t , we encode each Gaussian with a feature of the same dimensionality. This tests whether the encoding strategy is essential for balancing representational capacity and computational efficiency.

(2) Number of Dynamic Fields F in Eq. 4. We vary $F \in \{1, 4, 8, 16\}$ and use $F = 8$ in the comparative experiment. This ablation validates our claim that F fields suffice to capture diverse yet structured dynamics.

(3) Neural ODEs Dynamics Evolver. We replace Neural ODEs with MLPs with the same number of parameters. This aims to validate the benefits of dynamics modeling in learning physical dynamics.

(4) Effect of Physical Decoding (PD) in Eq. 10. We remove Rodrigues' rotation formula [46] to update the motion. This tests whether physically meaningful transformations help maintain physically plausible motion.

(5) Removing Progressive Training (PT). We disable the deformation warm-up to align with existing methods. This evaluates the importance of progressive training in disentangling geometry and dynamics.

(6) Removing Neighborhood Regularization (NR). We compute the neighborhood graph once and cache it throughout training. This tests whether online updating neighborhood partitions enhances model robustness.

Results & Analysis: Tab. 4 shows that: **(1)** Removing

the factorized encoding significantly increases GPU memory consumption even on object-level 3D scenes, while bringing no performance improvement. Since motion exhibits correlation, assigning an independent dynamic state to each particle not only greatly increases computational complexity but also slightly degrades performance. This demonstrates that our factorized encoding is crucial for striking a balance between computational efficiency and representational capacity. **(2)** Using too few dynamic feature fields ($F = 1$) leads to a noticeable performance drop, while increasing F beyond a moderate number ($F = 16$) yields limited gains. This suggests that a sufficient yet compact set of dynamic feature fields is sufficient to capture the regular motion patterns. **(3)** Replacing Neural ODE-based Dynamics Evolver with MLPs causes the largest performance degradation. Since the dynamics typically follow high-order, continuous differential equations, Neural ODEs are inherently more suitable for modeling such dynamics. This confirms the necessity of introducing Neural ODEs into our framework. **(4)** Removing the physically meaningful decoding formulation noticeably reduces extrapolation accuracy, indicating that the physically consistent decoding process helps the model learn realistic dynamic behaviors. **(5–6)** Excluding either the progressive training or the neighborhood regularization leads to lower performance, verifying that these strategies improve the robustness of the proposed ParticleGS model.

5. Conclusion

We introduce ParticleGS, a dynamic 3DGS method that learns neural dynamics directly from video observations. By modeling physical states and learning state transition laws, ParticleGS ensures stable extrapolation. Experimental results demonstrate that ParticleGS outperforms existing baselines across multiple benchmarks.

Limitations. Similar to other methods, ParticleGS currently cannot predict motions that deviate from the physical dynamics observed during training (e.g., sudden object breakage), as it has not learned to model such behaviors.

References

[1] Jeongmin Bae, Seoha Kim, Youngsik Yun, Hahyun Lee, Gun Bang, and Youngjung Uh. Per-gaussian embedding-based deformation for deformable 3d gaussian splatting. In *European Conference on Computer Vision*, pages 321–335. Springer, 2024. [2](#)

[2] Junhao Cai, Yuji Yang, Weihao Yuan, Yisheng He, Zilong Dong, Liefeng Bo, Hui Cheng, and Qifeng Chen. Gic: Gaussian-informed continuum for physical property identification and simulation. In *Advances in Neural Information Processing Systems*, pages 75035–75063, 2024. [2](#)

[3] Ang Cao and Justin Johnson. Hexplane: A fast representation for dynamic scenes. In *Proceedings of the IEEE/CVF Conference on Computer Vision and Pattern Recognition*, pages 130–141, 2023. [1, 2, 5, 6](#)

[4] Junyi Cao, Shanyan Guan, Yanhao Ge, Wei Li, Xiaokang Yang, and Chao Ma. Neuma: Neural material adaptor for visual grounding of intrinsic dynamics. *Advances in Neural Information Processing Systems*, 37:65643–65669, 2024. [1, 2](#)

[5] Yadi Cao, Menglei Chai, Minchen Li, and Chenfanfu Jiang. Efficient learning of mesh-based physical simulation with bi-stride multi-scale graph neural network. In *International conference on machine learning*, pages 3541–3558. PMLR, 2023. [2](#)

[6] Ricky TQ Chen, Yulia Rubanova, Jesse Bettencourt, and David K Duvenaud. Neural ordinary differential equations. *Advances in Neural Information Processing Systems*, 31, 2018. [2, 4](#)

[7] Mengyu Chu, Lingjie Liu, Quan Zheng, Erik Franz, Hans-Peter Seidel, Christian Theobalt, and Rhaleb Zayer. Physics informed neural fields for smoke reconstruction with sparse data. *ACM Transactions on Graphics*, 41(4):1–14, 2022. [1, 2](#)

[8] Salvatore Cuomo, Vincenzo Schiano Di Cola, Fabio Giampaolo, Gianluigi Rozza, Maziar Raissi, and Francesco Piccialli. Scientific machine learning through physics-informed neural networks: Where we are and what’s next. *Journal of Scientific Computing*, 92(3):88, 2022. [1](#)

[9] Gilles Daviet, Tianchang Shen, Nicholas Sharp, and David IW Levin. Neurally integrated finite elements for differentiable elasticity on evolving domains. *ACM Transactions on Graphics*, 2024. [1](#)

[10] Filipe de Avila Belbute-Peres, Kevin Smith, Kelsey Allen, Josh Tenenbaum, and J Zico Kolter. End-to-end differentiable physics for learning and control. *Advances in neural information processing systems*, 31, 2018. [2](#)

[11] Tao Du, Kui Wu, Pingchuan Ma, Sebastien Wah, Andrew Spielberg, Daniela Rus, and Wojciech Matusik. Diffpd: Differentiable projective dynamics. *ACM Transactions on Graphics*, 41(2):1–21, 2021. [2](#)

[12] Jiemin Fang, Taoran Yi, Xinggang Wang, Lingxi Xie, Xiaopeng Zhang, Wenyu Liu, Matthias Nießner, and Qi Tian. Fast dynamic radiance fields with time-aware neural voxels. In *SIGGRAPH Asia 2022 Conference Papers*, pages 1–9, 2022. [1, 2, 5, 6](#)

[13] Yutao Feng, Yintong Shang, Xuan Li, Tianjia Shao, Chenfanfu Jiang, and Yin Yang. Pie-nerf: Physics-based interactive elastodynamics with nerf. In *Proceedings of the IEEE/CVF Conference on Computer Vision and Pattern Recognition*, pages 4450–4461, 2024. [1, 2](#)

[14] Sara Fridovich-Keil, Giacomo Meanti, Frederik Rahbæk Warburg, Benjamin Recht, and Angjoo Kanazawa. K-planes: Explicit radiance fields in space, time, and appearance. In *Proceedings of the IEEE/CVF Conference on Computer Vision and Pattern Recognition*, pages 12479–12488, 2023. [2](#)

[15] Shanyan Guan, Huayu Deng, Yunbo Wang, and Xiaokang Yang. Neurofluid: Fluid dynamics grounding with particle-driven neural radiance fields. In *International Conference on Machine Learning*, pages 7919–7929, 2022. [1, 2](#)

[16] Minghao Guo, Bohan Wang, Pingchuan Ma, Tianyuan Zhang, Crystal Owens, Chuang Gan, Josh Tenenbaum, Kaiming He, and Wojciech Matusik. Physically compatible 3d object modeling from a single image. *Advances in Neural Information Processing Systems*, 37:119260–119282, 2024. [1, 2](#)

[17] Zhongkai Hao, Chengyang Ying, Hang Su, Jun Zhu, Jian Song, and Ze Cheng. Bi-level physics-informed neural networks for pde constrained optimization using broyden’s hypergradients. In *International Conference on Learning Representations*, 2023. [2](#)

[18] Yi-Hua Huang, Yang-Tian Sun, Ziyi Yang, Xiaoyang Lyu, Yan-Pei Cao, and Xiaojuan Qi. Sc-gs: Sparse-controlled gaussian splatting for editable dynamic scenes. In *Proceedings of the IEEE/CVF Conference on Computer Vision and Pattern Recognition*, pages 4220–4230, 2024. [2](#)

[19] Woobin Im, Geonho Cha, Sebin Lee, Jumin Lee, Juhyeong Seon, Dongyoon Wee, and Sung-Eui Yoon. Regularizing dynamic radiance fields with kinematic fields. In *European Conference on Computer Vision*, pages 312–328. Springer, 2024. [2](#)

[20] Boyan Jiang, Yinda Zhang, Xingkui Wei, Xiangyang Xue, and Yanwei Fu. Learning compositional representation for 4d captures with neural ode. In *Proceedings of the IEEE/CVF Conference on Computer Vision and Pattern Recognition*, pages 5340–5350, 2021. [2](#)

[21] Kai Katsumata, Duc Minh Vo, and Hideki Nakayama. A compact dynamic 3d gaussian representation for real-time dynamic view synthesis. In *European Conference on Computer Vision*, pages 394–412. Springer, 2024. [2](#)

[22] Bernhard Kerbl, Georgios Kopanas, Thomas Leimkühler, and George Drettakis. 3d gaussian splatting for real-time radiance field rendering. *ACM TRANSACTIONS ON GRAPHICS*, 42(4):139–1, 2023. [2, 3, 5](#)

[23] Agelos Kratimenos, Jiahui Lei, and Kostas Daniilidis. Dynmf: Neural motion factorization for real-time dynamic view synthesis with 3d gaussian splatting. In *European Conference on Computer Vision*, pages 252–269. Springer, 2024. [2](#)

[24] Wilhelm Kutta. *Beitrag zur näherungsweisen Integration totaler Differentialgleichungen*. Teubner, 1901. [5](#)

[25] Jinxi Li, Ziyang Song, and Bo Yang. Nvfi: Neural velocity fields for 3d physics learning from dynamic videos.

Advances in Neural Information Processing Systems, 36: 34723–34751, 2023. 1, 2, 5, 6

[26] Jinxi Li, Ziyang Song, and Bo Yang. Trace: Learning 3d gaussian physical dynamics from multi-view videos. *ICCV*, 2025. 2, 5, 6

[27] Jinxi Li, Ziyang Song, Siyuan Zhou, and Bo Yang. Free-gave: 3d physics learning from dynamic videos by gaussian velocity. In *Proceedings of the Computer Vision and Pattern Recognition Conference*, pages 12433–12443, 2025. 2, 5, 6

[28] Xuan Li, Yi-Ling Qiao, Peter Yichen Chen, Krishna Murthy Jatavallabhula, Ming Lin, Chenfanfu Jiang, and Chuang Gan. Pac-nerf: Physics augmented continuum neural radiance fields for geometry-agnostic system identification. In *International Conference on Learning Representations*, 2023. 2

[29] Yifei Li, Hsiao-yu Chen, Egor Larionov, Nikolaos Sarafianos, Wojciech Matusik, and Tuur Stuyck. Diffavatar: Simulation-ready garment optimization with differentiable simulation. In *Proceedings of the IEEE/CVF Conference on Computer Vision and Pattern Recognition*, pages 4368–4378, 2024. 2

[30] Junbang Liang and Ming C Lin. Differentiable physics simulation. In *ICLR 2020 Workshop on Integration of Deep Neural Models and Differential Equations*, 2020. 2

[31] Jiajing Lin, Shu Jiang, Qingyuan Zeng, Zhenzhong Wang, and Min Jiang. Visionlaw: Inferring interpretable intrinsic dynamics from visual observations via bilevel optimization. *ArXiv:2508.13792*, 2025. 2

[32] Youtian Lin, Zuozhuo Dai, Siyu Zhu, and Yao Yao. Gaussian-flow: 4d reconstruction with dynamic 3d gaussian particle. In *Proceedings of the IEEE/CVF Conference on Computer Vision and Pattern Recognition*, pages 21136–21145, 2024. 2

[33] Yuchen Lin, Chenguo Lin, Jianjin Xu, and Yadong MU. OmniphysGS: 3d constitutive gaussians for general physics-based dynamics generation. In *International Conference on Learning Representations*, 2025. 1, 2

[34] Shaowei Liu, Zhongzheng Ren, Saurabh Gupta, and Shenglong Wang. Physgen: Rigid-body physics-grounded image-to-video generation. In *European Conference on Computer Vision*, pages 360–378. Springer, 2024. 2

[35] Jonathon Luiten, Georgios Kopanas, Bastian Leibe, and Deva Ramanan. Dynamic 3d gaussians: Tracking by persistent dynamic view synthesis. In *International Conference on 3D Vision*, pages 800–809. IEEE, 2024. 2

[36] Pingchuan Ma, Peter Yichen Chen, Bolei Deng, Joshua B Tenenbaum, Tao Du, Chuang Gan, and Wojciech Matusik. Learning neural constitutive laws from motion observations for generalizable pde dynamics. In *International Conference on Machine Learning*, pages 23279–23300. PMLR, 2023. 2

[37] Shaojie Ma, Yawei Luo, and Yi Yang. Reconstructing and simulating dynamic 3d objects with mesh-adsorbed gaussian splatting. *ArXiv:2406.01593*, 2024. 2

[38] Qiaowei Miao, Kehan Li, Jinsheng Quan, Zhiyuan Min, Shaojie Ma, Yichao Xu, Yi Yang, and Yawei Luo. Advances in 4d generation: A survey. *ArXiv:2503.14501*, 2025. 1

[39] Ben Mildenhall, Pratul P Srinivasan, Matthew Tancik, Jonathan T Barron, Ravi Ramamoorthi, and Ren Ng. Nerf: Representing scenes as neural radiance fields for view synthesis. *Communications of the ACM*, 65(1):99–106, 2021. 2

[40] Thomas Müller, Alex Evans, Christoph Schied, and Alexander Keller. Instant neural graphics primitives with a multiresolution hash encoding. *ACM transactions on graphics*, 41(4):1–15, 2022. 2

[41] Michael Niemeyer, Lars Mescheder, Michael Oechsle, and Andreas Geiger. Occupancy flow: 4d reconstruction by learning particle dynamics. In *Proceedings of the IEEE/CVF International Conference on Computer Vision*, pages 5379–5389, 2019. 2

[42] Keunhong Park, Utkarsh Sinha, Jonathan T Barron, Sofien Bouaziz, Dan B Goldman, Steven M Seitz, and Ricardo Martin-Brualla. Nerfies: Deformable neural radiance fields. In *Proceedings of the IEEE/CVF international conference on computer vision*, pages 5865–5874, 2021. 2

[43] Albert Pumarola, Enric Corona, Gerard Pons-Moll, and Francesc Moreno-Noguer. D-nerf: Neural radiance fields for dynamic scenes. In *Proceedings of the IEEE/CVF Conference on Computer Vision and Pattern Recognition*, pages 10318–10327, 2021. 1, 2

[44] Charles Ruizhongtai Qi, Li Yi, Hao Su, and Leonidas J Guibas. Pointnet++: Deep hierarchical feature learning on point sets in a metric space. *Advances in neural information processing systems*, 30, 2017. 4

[45] Maziar Raissi, Paris Perdikaris, and George E Karniadakis. Physics-informed neural networks: A deep learning framework for solving forward and inverse problems involving nonlinear partial differential equations. *Journal of Computational physics*, 378:686–707, 2019. 1, 2

[46] Olinde Rodrigues. Des lois géométriques qui régissent les déplacements d'un système solide dans l'espace, et de la variation des coordonnées provenant de ces déplacements considérés indépendants des causes qui peuvent les produire. *Journal de Mathématiques Pures et Appliquées*, 1840. 5, 8

[47] Alvaro Sanchez-Gonzalez, Jonathan Godwin, Tobias Pfaff, Rex Ying, Jure Leskovec, and Peter Battaglia. Learning to simulate complex physics with graph networks. In *International conference on machine learning*, pages 8459–8468. PMLR, 2020. 2

[48] Johannes L Schonberger and Jan-Michael Frahm. Structure-from-motion revisited. In *Proceedings of the IEEE conference on computer vision and pattern recognition*, pages 4104–4113, 2016. 3

[49] Ruizhi Shao, Zerong Zheng, Hanzhang Tu, Boning Liu, Hongwen Zhang, and Yebin Liu. Tensor4d: Efficient neural 4d decomposition for high-fidelity dynamic reconstruction and rendering. In *Proceedings of the IEEE/CVF Conference on Computer Vision and Pattern Recognition*, pages 16632–16642, 2023. 2

[50] Ramansh Sharma and Varun Shankar. Accelerated training of physics-informed neural networks (pinns) using meshless discretizations. *Advances in neural information processing systems*, 35:1034–1046, 2022. 1

[51] Alexey Stomakhin, Craig Schroeder, Lawrence Chai, Joseph Teran, and Andrew Selle. A material point method for snow

simulation. *ACM Transactions on Graphics*, 32(4):1–10, 2013. [4](#)

[52] Jiakai Sun, Han Jiao, Guangyuan Li, Zhanjie Zhang, Lei Zhao, and Wei Xing. 3dstream: On-the-fly training of 3d gaussians for efficient streaming of photo-realistic free-viewpoint videos. In *Proceedings of the IEEE/CVF Conference on Computer Vision and Pattern Recognition*, pages 20675–20685, 2024. [2](#)

[53] Yuqi Wang, Jiawei He, Lue Fan, Hongxin Li, Yuntao Chen, and Zhaoxiang Zhang. Driving into the future: Multiview visual forecasting and planning with world model for autonomous driving. In *Proceedings of the IEEE/CVF Conference on Computer Vision and Pattern Recognition*, pages 14749–14759, 2024. [1](#)

[54] Guanjun Wu, Taoran Yi, Jiemin Fang, Lingxi Xie, Xiaopeng Zhang, Wei Wei, Wenyu Liu, Qi Tian, and Xinggang Wang. 4d gaussian splatting for real-time dynamic scene rendering. In *Proceedings of the IEEE/CVF Conference on Computer Vision and Pattern Recognition*, pages 20310–20320, 2024. [1, 2, 3, 5](#)

[55] Jiahao Wu, Rui Peng, Zhiyan Wang, Lu Xiao, Luyang Tang, Jinbo Yan, Kaiqiang Xiong, and Ronggang Wang. Swift4d: Adaptive divide-and-conquer gaussian splatting for compact and efficient reconstruction of dynamic scene. In *International Conference on Learning Representations*, 2025. [2](#)

[56] Tianyi Xie, Zeshun Zong, Yuxing Qiu, Xuan Li, Yutao Feng, Yin Yang, and Chenfanfu Jiang. Physgaussian: Physics-integrated 3d gaussians for generative dynamics. In *Proceedings of the IEEE/CVF Conference on Computer Vision and Pattern Recognition*, pages 4389–4398, 2024. [1, 2](#)

[57] Xiaoyu Xiong, Changyu Hu, Chunru Lin, Pingchuan Ma, Chuang Gan, and Tao Du. Topogaussian: Inferring internal topology structures from visual clues. *International Conference on Learning Representations*, 2025. [2](#)

[58] Jiawei Xu, Zexin Fan, Jian Yang, and Jin Xie. Grid4d: 4d decomposed hash encoding for high-fidelity dynamic gaussian splatting. *Advances in Neural Information Processing Systems*, 37:123787–123811, 2024. [1, 2, 3, 5, 6](#)

[59] Ziyi Yang, Xinyu Gao, Wen Zhou, Shaohui Jiao, Yuqing Zhang, and Xiaogang Jin. Deformable 3d gaussians for high-fidelity monocular dynamic scene reconstruction. In *Proceedings of the IEEE/CVF Conference on Computer Vision and Pattern Recognition*, pages 20331–20341, 2024. [1, 2, 3, 5, 6](#)

[60] Hang Yin, Anastasia Varava, and Danica Kragic. Modeling, learning, perception, and control methods for deformable object manipulation. *Science Robotics*, 6(54):eabd8803, 2021. [1](#)

[61] Boming Zhao, Yuan Li, Ziyu Sun, Lin Zeng, Yujun Shen, Rui Ma, Yinda Zhang, Hujun Bao, and Zhaopeng Cui. Gaus-sianprediction: Dynamic 3d gaussian prediction for motion extrapolation and free view synthesis. In *ACM SIGGRAPH 2024 Conference Papers*, pages 1–12, 2024. [1, 2, 5, 6](#)

[62] Licheng Zhong, Hong-Xing Yu, Jiajun Wu, and Yunzhu Li. Reconstruction and simulation of elastic objects with spring-mass 3d gaussians. In *European Conference on Computer Vision*, pages 407–423. Springer, 2024. [2](#)

[63] Yaofeng Desmond Zhong, Biswadip Dey, and Amit Chakraborty. Symplectic ode-net: Learning hamiltonian dynamics with control. In *International Conference on Learning Representations*, 2020. [2](#)

ParticleGS: Learning Neural Gaussian Particle Dynamics from Videos for Prior-free Physical Motion Extrapolation

Supplementary Material

The appendix includes:

- A Toy Experiment: Learning Dynamics vs. Memorizing Trajectories.
- Implementation Details.
- Additional Qualitative Comparisons.
- Full Quantitative Results.

6. A Toy Experiment: Learning Dynamics vs. Memorizing Trajectories

To intuitively understand the limitations of time-conditioned representations and the necessity of our physics-based approach, we conducted a toy experiment on a 2D damped harmonic oscillator system (a spiral trajectory), as shown in Fig. 6. We trained two models on the initial segment of the spiral (corrupted by random noise, indicated by green dots) and tested their ability to predict the future evolution (indicated by red dots).

Analysis of Time-Conditioned Models. As illustrated in Fig. 6(a), the baseline method, which models position as a direct function of time ($x = \mathcal{F}(t)$), successfully interpolates the training points. However, it fails to extrapolate to the future. This is because the baseline essentially performs curve fitting on the time coordinate, memorizing the correlation between a specific timestamp t and a position x within the observed window. Once t extends beyond this range, the network lacks the underlying physical context to predict the future, reverting to linear behavior that violates the system’s inherent dynamics.

Analysis of Neural ODEs. In contrast, Fig. 6(b) demonstrates that the Neural ODE-based approach accurately predicts the future spiral motion. This success stems from the fact that Neural ODEs do not map time directly to position. Instead, they approximate the governing equation of the system: $\frac{dx}{dt} = f(x, t)$. While the position $x(t)$ changes constantly, the physical law f governing the change remains consistent. By learning this derivative function from the observed past, the model can integrate the same law to generate physically plausible future states. This observation motivates ParticleGS to move from memorizing temporal deformations to learning the physical laws driving the system.

7. Implementation Details

Input Representation. To capture the comprehensive state of each Gaussian particle, we construct a 14-dimensional feature vector as the input to our network. Specifically, this vector is a concatenation of the position $x \in \mathbb{R}^3$, rotation

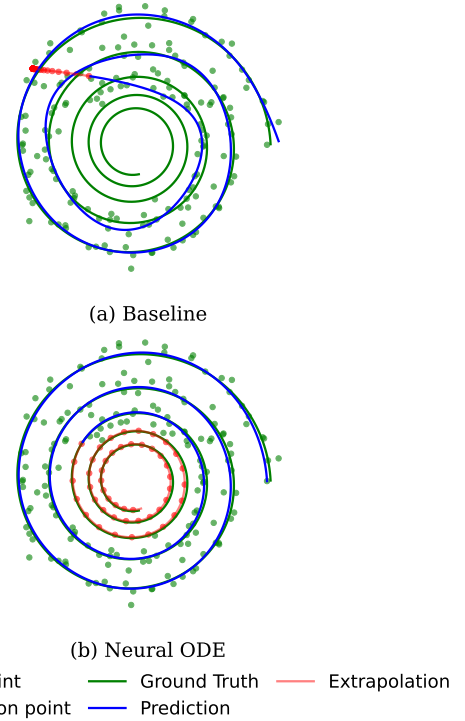


Figure 6. **Toy experiment on extrapolation capabilities.** We visualize the predicted trajectories on a 2D damped spiral. Green dots represent observed training data, while red dots indicate the unobserved future. **(a) Baseline:** The time-conditioned baseline fits the training data well but fails during extrapolation, producing a linear trajectory that deviates from the physical spiral. **(b) Neural ODE:** By modeling the underlying derivatives, the Neural ODE accurately captures the spiral dynamics, maintaining the correct trajectory even in the unobserved region.

quaternion $r \in \mathbb{R}^4$, scaling $s \in \mathbb{R}^3$, opacity $\alpha \in \mathbb{R}^1$, and the 0-th order of the Spherical Harmonics coefficients $sh \in \mathbb{R}^3$. This compact representation enables the encoder to extract both geometric and photometric cues effectively.

Dynamics Latent Space Encoder f_{encoder} : The encoder is designed to extract particle-level static features and system-level dynamic fields. It consists of 4 stacked attention layers, each with a hidden dimension of 256, employing GELU as the activation function. To handle the unstructured nature of 3D Gaussian clouds, we construct local Gaussian patches using Farthest Point Sampling (FPS) and k -nearest neighbors (k-NN). We employ FPS to select representative anchor points from the Gaussian cloud. For synthetic datasets, we sample $N_k = 2048$ keypoints. For

real-world datasets which typically contain more complex geometries and background noise, we increase the sampling density to $N_k = 4096$. For each keypoint, we query its $k = 32$ nearest neighbors (k-NN) based on Euclidean distance to form a local patch. To adapt to the changing Gaussian distribution, we regenerate these neighborhood patches immediately after every densification step or at a fixed interval of 500 iterations.

This hierarchical design ensures efficient information aggregation across the scene.

Neural ODE Dynamics Evolver f_{evolver} : The evolver is the core component for modeling continuous-time dynamics. We implement f_{evolver} using a network composed of two stacked 3-layer MLP blocks equipped with residual connections to facilitate gradient flow. All hidden layers maintain a dimension of 128 and use GELU activation. We utilize the Runge-Kutta 4 (RK4) method as the ODE solver to integrate the learned derivative function.

Gaussian Kernel Space Decoder f_{decoder} : We use a 6-layer MLP with a hidden dimension of 256 for all layers, using GELU as the activation function.

Physical State Dimensions. We set the dimension of the static features L to 16 and the dimension of each dynamic field G to 16.

Optimization. We train our framework using the Adam optimizer and adopt a progressive training strategy. The total training iterations are set to 40,000 for synthetic datasets and 60,000 for real-world datasets. For 0-3k iterations: We adopt Geometry Warm-up and optimize only the static Gaussian parameters to obtain a reliable canonical geometry. For 3k-7k iterations: We adopt Dynamics Warm-up, where we freeze the canonical Gaussians and optimize the ParticleGS network with a gradually increasing temporal window. For 7k-40k/60k iterations: Both the canonical Gaussians and the neural networks are jointly optimized to refine fine-grained details until the end of training.

8. Rodrigues' Rotation Formula

In our framework, the decoder predicts a rotation vector $R \in \mathbb{R}^3$ (representing the axis-angle notation) to model the rotational dynamics. To apply this rotation to the 3D Gaussians, we convert R into a valid rotation matrix $\text{Rod}(R) \in \mathbb{R}^{3 \times 3}$ using Rodrigues' rotation formula. Given the rotation vector $R = [r_x, r_y, r_z]^T$, the rotation angle θ is defined as its Euclidean norm:

$$\theta = \|R\|_2. \quad (13)$$

If θ is non-zero, the normalized rotation axis $K = [k_x, k_y, k_z]^T$ is computed as $K = R/\theta$. We first define the skew-symmetric matrix $[K]_\times$ associated with the unit

vector K :

$$[K]_\times = \begin{bmatrix} 0 & -k_z & k_y \\ k_z & 0 & -k_x \\ -k_y & k_x & 0 \end{bmatrix}. \quad (14)$$

Rodrigues' rotation formula then expresses the rotation matrix $\text{Rod}(R)$ as:

$$\text{Rod}(R) = I + \sin \theta [K]_\times + (1 - \cos \theta) [K]_\times^2, \quad (15)$$

where I is the 3×3 identity matrix.

9. Additional Qualitative Comparisons

We provide additional visual comparisons across various datasets in Fig. 7 through Fig. 12. The **red bounding boxes** in the figures mark the regions with ground truth motion, serving as a visual reference for the object's actual position and movement trajectory. The **bottom section** of each sub-figure displays details of specific regions.

10. Full Quantitative Results

We report the complete quantitative results for both reconstruction and extrapolation tasks. Detailed metrics, including PSNR, SSIM, and LPIPS, are provided for every scene in the datasets to ensure a thorough evaluation.

10.1. Full Results on Dynamic Object Dataset

Table 5 presents the detailed quantitative comparisons on the Dynamic Object Dataset, which includes scenes such as Falling Ball, Bat, Fan, Telescope, Shark, and Whale.

10.2. Full Results on Dynamic Indoor Scene Dataset

The results for the Dynamic Indoor Scene Dataset are summarized in Table 6. This dataset features complex background geometries and lighting conditions, represented by scenes like Gnome House, Chessboard, Factory, and Dining Table.

10.3. Full Results on Dynamic Multipart Dataset

We also evaluate our method on the Dynamic Multipart Dataset, which includes objects exhibiting distinct part-level motion patterns, such as Folding Chair, Satellite, Stove, and Hyperbolic. The full quantitative results are shown in Table 7.

10.4. Full Results on FreeGave-GoPro Dataset

Finally, Table 8 details the performance on the FreeGave-GoPro Dataset, covering real-world captured scenes such as Box, Collision, Wrist Rest, Hammer, and Pen.

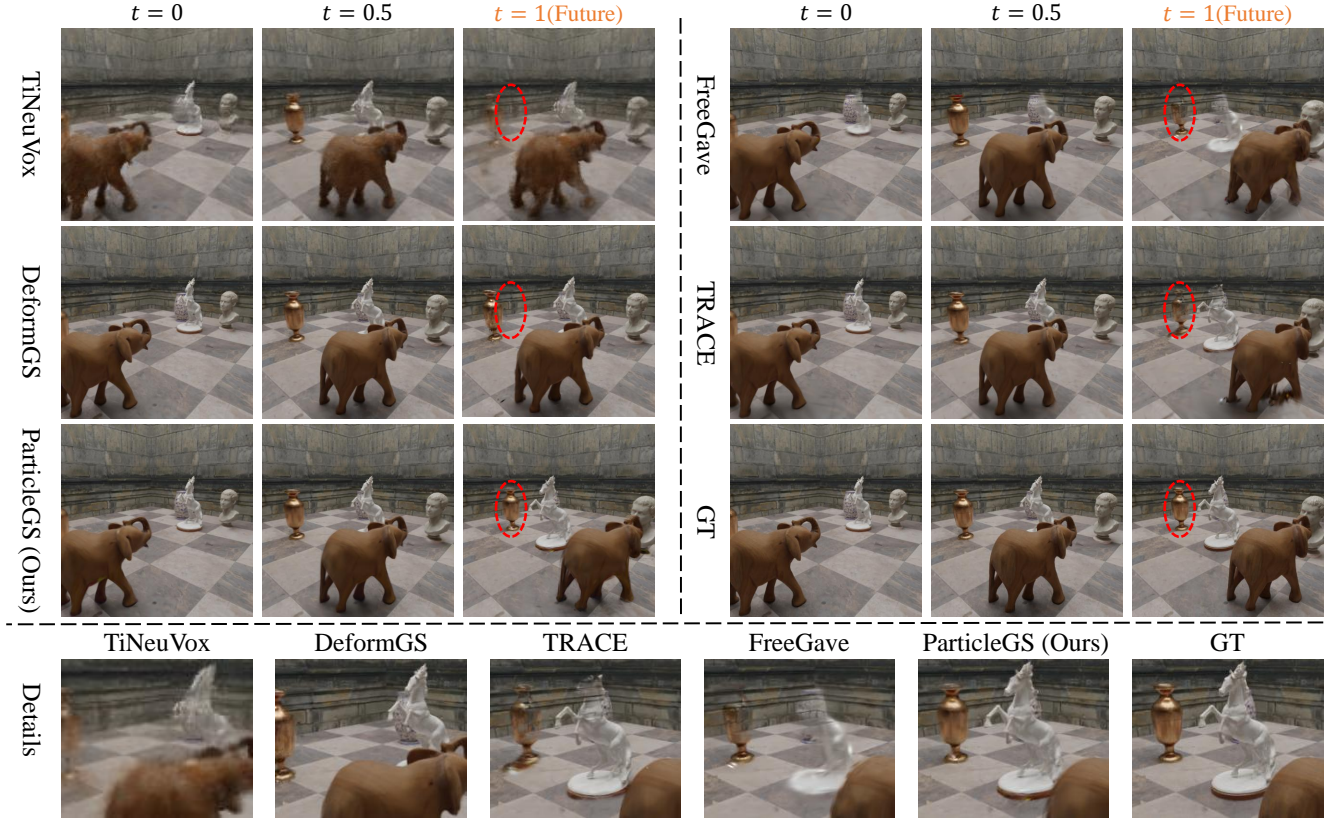


Figure 7. Additional qualitative comparisons on the Dynamic Indoor Scene Dataset.

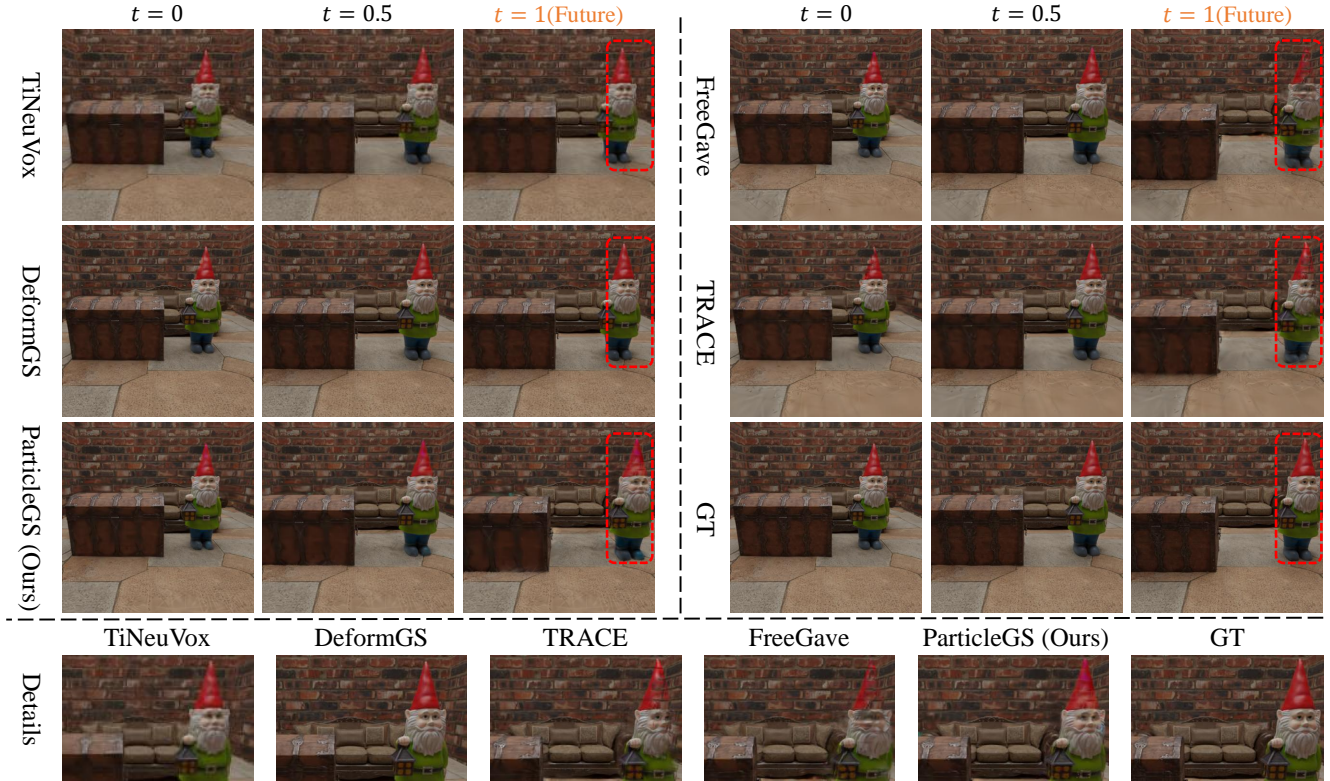


Figure 8. Additional qualitative comparisons on the Dynamic Indoor Scene Dataset.

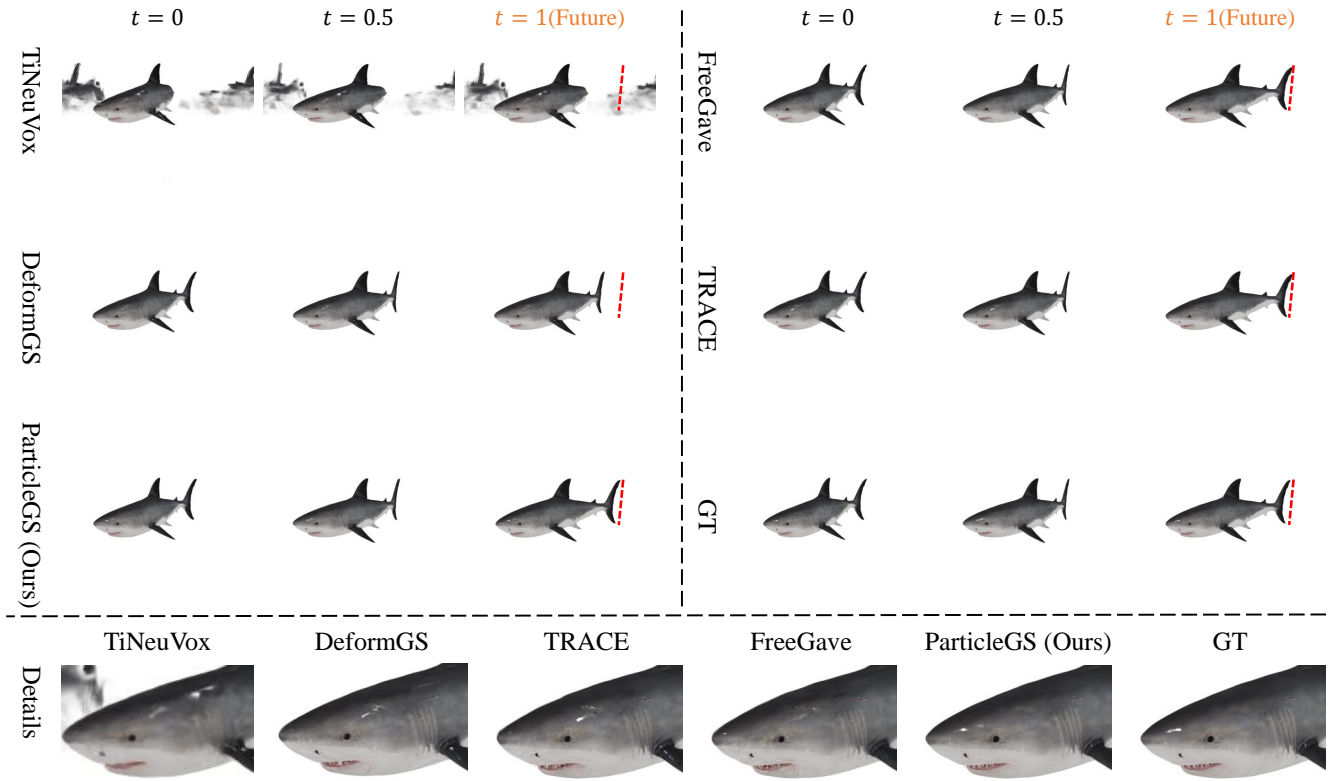


Figure 9. Additional qualitative comparisons on the Dynamic Object Dataset.

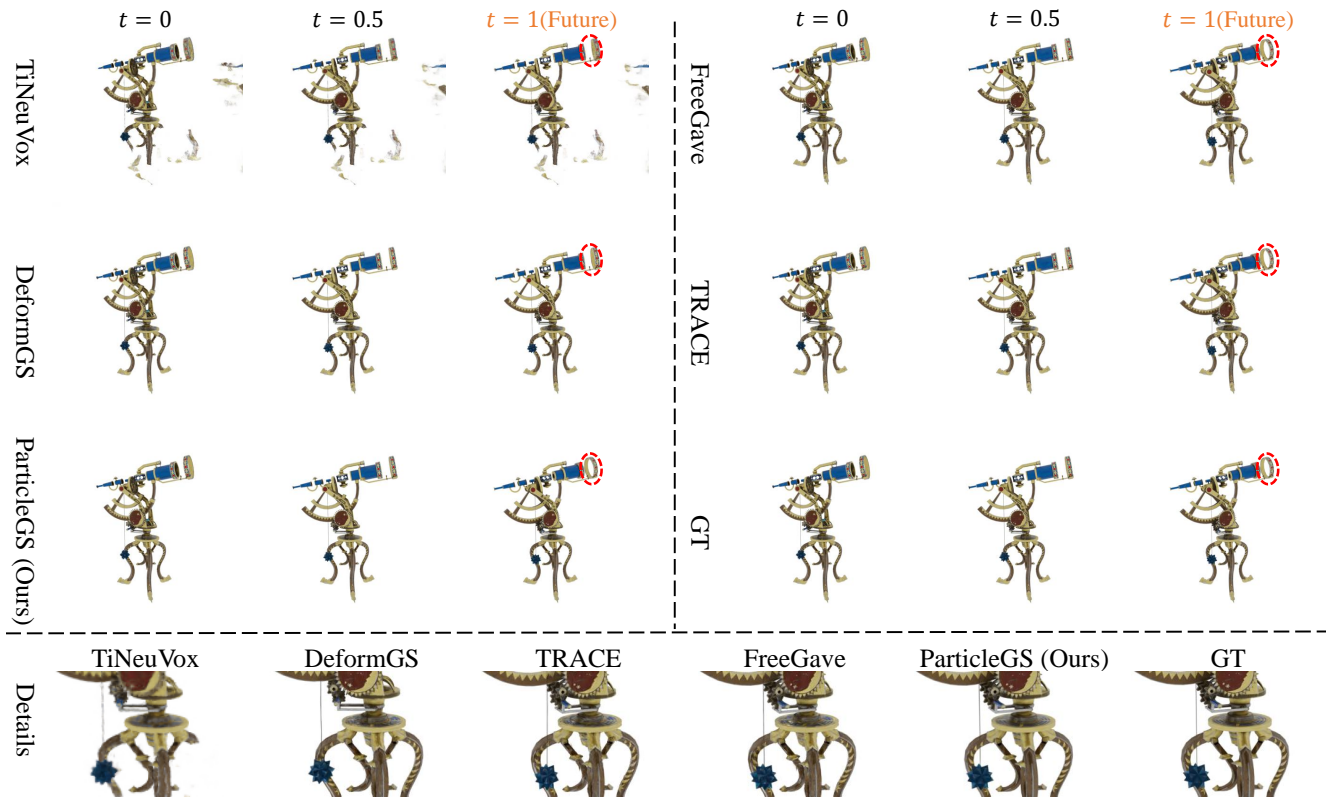


Figure 10. Additional qualitative comparisons on the Dynamic Object Dataset.

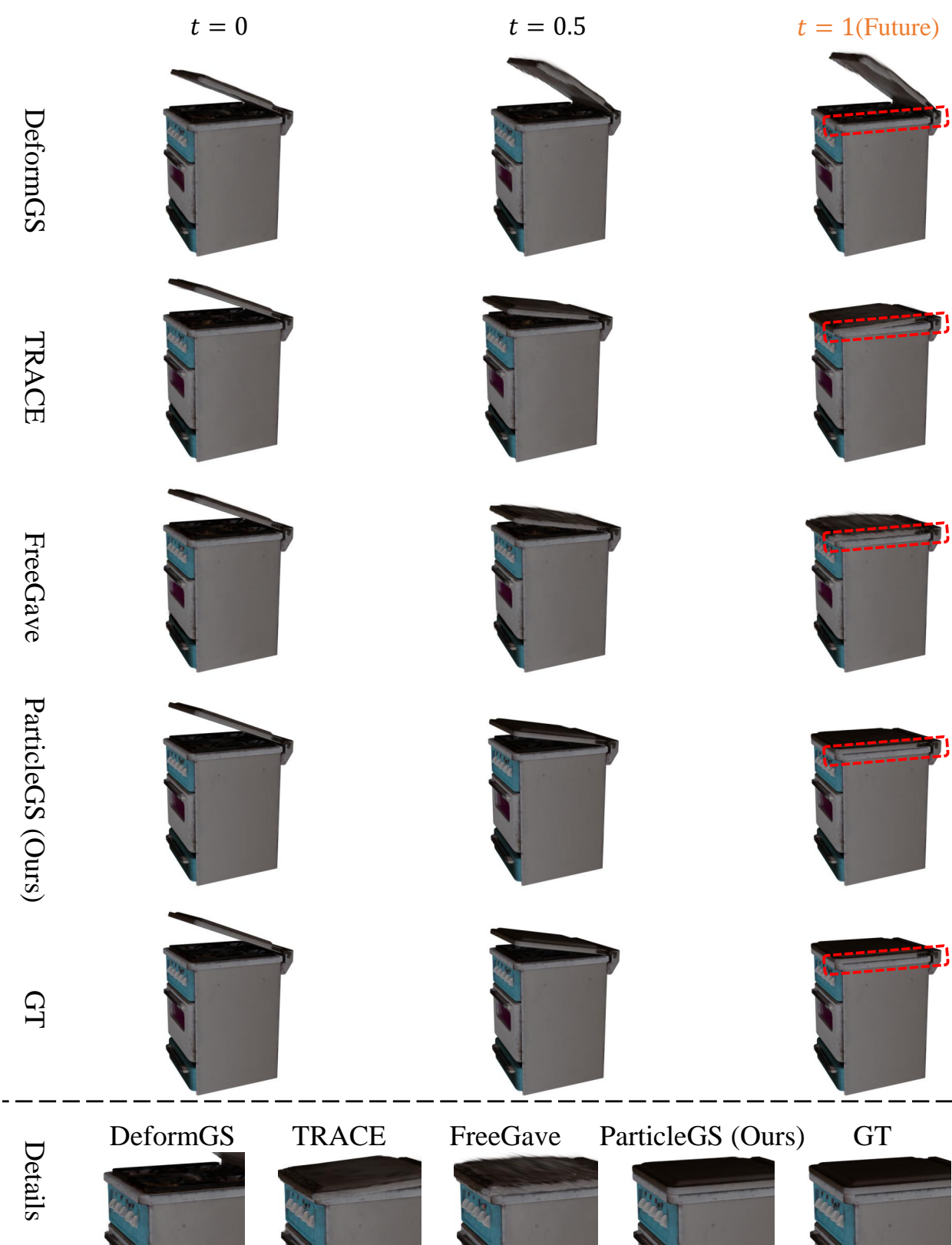


Figure 11. Additional qualitative comparisons on the Dynamic Multipart Dataset.

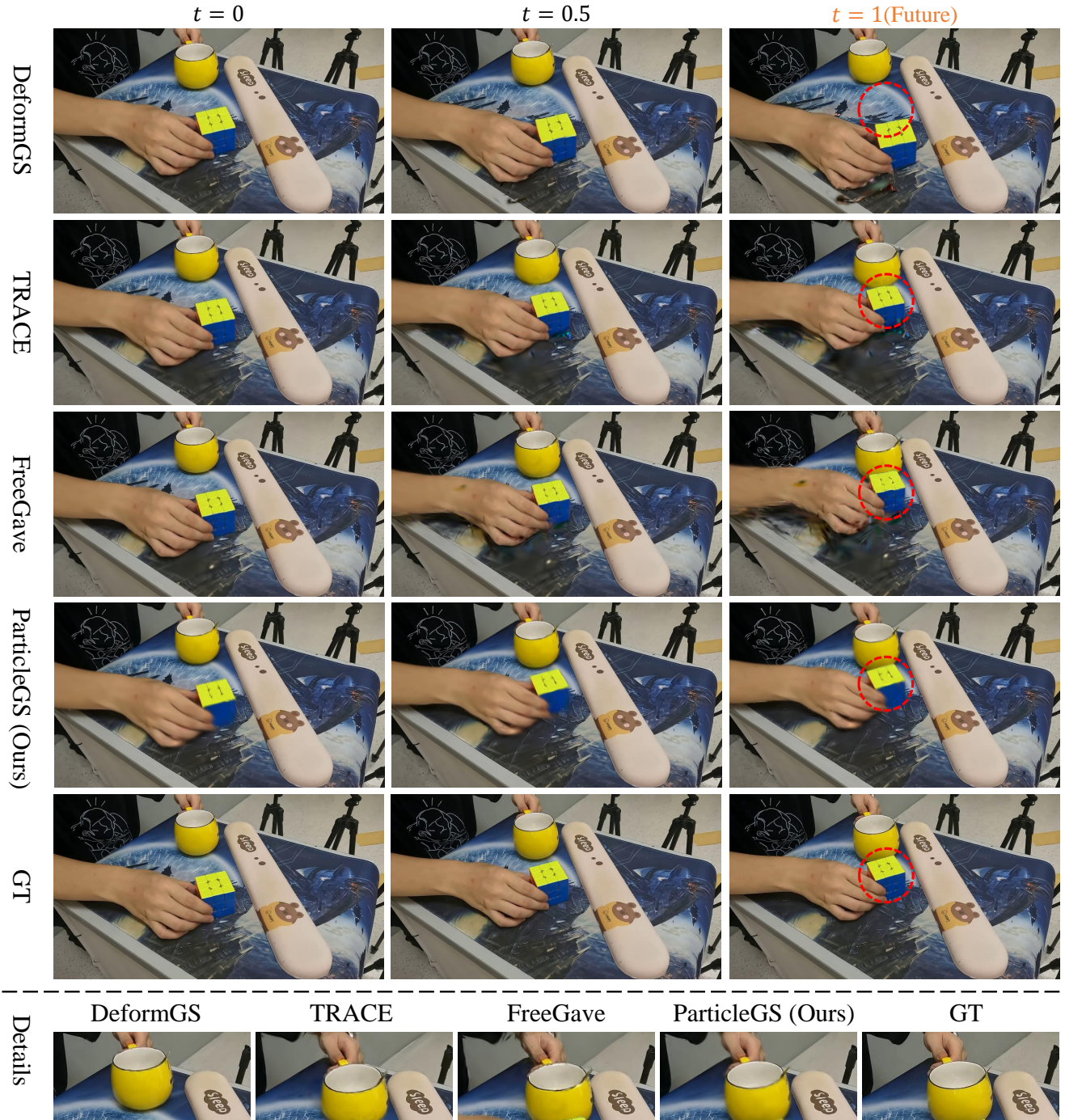


Figure 12. Additional qualitative comparisons on the FreeGave-GoPro Dataset

Table 5. Full quantitative results on the Dynamic Objects, rendered at the source resolution. **Bold** and underline indicate the best and second best performance.

Method	Falling Ball						Bat					
	Reconstruction			Extrapolation			Reconstruction			Extrapolation		
	PSNR↑	SSIM↑	LPIPS↓	PSNR↑	SSIM↑	LPIPS↓	PSNR↑	SSIM↑	LPIPS↓	PSNR↑	SSIM↑	LPIPS↓
HexPlane	19.754	0.816	0.215	20.166	0.906	0.130	22.099	0.953	0.080	22.422	0.954	0.061
TiNeuVox	24.323	0.894	0.167	20.474	0.940	0.098	17.611	0.946	0.076	17.139	0.947	0.070
DeformGS	17.736	0.830	0.156	26.384	0.945	0.060	<u>47.034</u>	<u>0.996</u>	0.004	27.109	0.944	0.034
Grid4D	19.119	0.821	0.153	24.926	0.925	0.069	47.443	0.997	0.004	29.551	0.953	0.290
NVF	34.900	0.969	0.068	27.013	0.966	0.074	24.648	0.970	0.044	25.529	0.973	0.040
GSPrediction	24.549	0.910	0.154	16.790	0.830	0.238	43.290	0.997	0.002	23.495	0.952	0.075
TRACE	<u>41.077</u>	<u>0.995</u>	0.017	38.126	<u>0.993</u>	0.020	39.269	0.995	0.006	28.890	<u>0.982</u>	0.016
FreeGave	42.248	0.996	<u>0.015</u>	37.460	0.994	<u>0.015</u>	39.516	0.995	0.006	<u>30.907</u>	0.980	<u>0.014</u>
ParticleGS	38.275	0.991	0.010	<u>38.067</u>	0.990	0.013	43.232	0.997	<u>0.003</u>	36.348	0.984	0.011

Method	Fan						Telescope					
	Reconstruction			Extrapolation			Reconstruction			Extrapolation		
	PSNR↑	SSIM↑	LPIPS↓	PSNR↑	SSIM↑	LPIPS↓	PSNR↑	SSIM↑	LPIPS↓	PSNR↑	SSIM↑	LPIPS↓
HexPlane	18.424	0.842	0.190	19.998	0.887	0.106	21.814	0.917	0.149	23.667	0.931	0.082
TiNeuVox	15.775	0.855	0.189	21.307	0.919	0.081	23.088	0.949	0.084	20.801	0.925	0.071
DeformGS	<u>38.083</u>	0.973	0.026	24.473	0.930	0.047	38.435	0.992	<u>0.005</u>	23.186	0.934	0.037
Grid4D	37.031	0.967	0.030	26.720	0.941	0.044	38.488	0.992	0.006	25.696	0.942	0.033
NVF	27.748	0.953	0.059	27.347	0.957	0.054	26.889	0.955	0.051	26.861	0.955	0.053
GSPrediction	34.864	<u>0.976</u>	0.020	20.747	0.935	0.054	36.191	0.992	0.004	22.018	0.939	0.043
TRACE	34.038	0.975	0.023	36.779	0.984	0.014	38.839	0.994	0.006	35.725	<u>0.980</u>	0.006
FreeGave	34.158	0.975	0.022	33.987	<u>0.974</u>	<u>0.016</u>	38.737	0.994	0.006	<u>36.407</u>	0.991	<u>0.005</u>
ParticleGS	38.852	0.979	<u>0.021</u>	<u>34.235</u>	<u>0.974</u>	0.023	<u>38.770</u>	<u>0.993</u>	0.004	38.294	0.991	0.004

Method	Shark						Whale					
	Reconstruction			Extrapolation			Reconstruction			Extrapolation		
	PSNR↑	SSIM↑	LPIPS↓	PSNR↑	SSIM↑	LPIPS↓	PSNR↑	SSIM↑	LPIPS↓	PSNR↑	SSIM↑	LPIPS↓
HexPlane	22.736	0.956	0.064	24.180	0.962	0.041	24.684	0.976	0.049	24.075	0.964	0.049
TiNeuVox	19.592	0.951	0.058	16.683	0.933	0.096	21.281	0.969	0.052	20.671	0.945	0.063
DeformGS	<u>40.492</u>	0.995	<u>0.008</u>	29.159	0.966	0.022	<u>42.475</u>	0.996	0.004	26.666	0.959	0.027
Grid4D	40.752	0.995	0.007	30.904	0.966	0.021	42.666	0.996	0.004	28.246	0.967	0.020
NVF	31.374	<u>0.982</u>	0.035	28.649	0.979	0.033	30.778	0.984	0.025	25.529	0.977	0.029
GSPrediction	40.015	0.995	0.010	30.280	0.971	0.032	39.540	0.996	<u>0.005</u>	25.596	0.965	0.046
TRACE	38.637	0.995	0.009	30.547	<u>0.982</u>	0.012	36.177	0.994	0.006	30.068	<u>0.980</u>	<u>0.013</u>
FreeGave	39.378	0.995	0.009	<u>31.639</u>	0.979	<u>0.011</u>	37.788	0.994	0.006	<u>31.395</u>	<u>0.980</u>	0.012
ParticleGS	40.322	0.995	<u>0.008</u>	37.475	0.983	0.010	39.241	0.995	<u>0.005</u>	34.236	0.983	0.012

Table 6. Full quantitative results on Dynamic Indoor Scene dataset, rendered at the source resolution. **Bold** and underline indicate the best and second best performance.

Method	Gnome House						Chessboard					
	Reconstruction			Extrapolation			Reconstruction			Extrapolation		
	PSNR↑	SSIM↑	LPIPS↓	PSNR↑	SSIM↑	LPIPS↓	PSNR↑	SSIM↑	LPIPS↓	PSNR↑	SSIM↑	LPIPS↓
HexPlane	18.060	0.419	0.650	23.341	0.601	0.530	18.054	0.515	0.617	22.034	0.680	0.500
TiNeuVox	24.644	0.663	0.385	21.359	0.665	0.357	<u>23.847</u>	<u>0.698</u>	0.392	20.088	0.676	0.408
DeformGS	21.855	0.611	<u>0.341</u>	22.728	0.731	<u>0.196</u>	20.688	0.659	0.443	20.484	0.773	0.280
Grid4D	22.418	0.588	0.360	21.185	0.696	0.258	21.545	0.667	0.437	19.713	0.741	0.331
NVFi	16.857	0.435	0.687	24.087	0.615	0.546	17.515	0.551	0.651	22.571	0.672	0.539
GSPrediction	16.113	0.556	0.632	20.098	0.641	0.371	17.665	0.651	0.470	20.033	0.724	0.317
TRACE	22.968	0.642	0.351	<u>29.325</u>	<u>0.840</u>	0.209	22.969	0.642	<u>0.352</u>	<u>29.326</u>	0.840	<u>0.209</u>
FreeGave	19.178	0.543	0.425	28.962	0.827	0.217	19.905	0.674	0.471	26.339	<u>0.862</u>	0.251
ParticleGS	24.481	<u>0.662</u>	0.307	31.167	0.843	0.160	25.449	0.785	0.287	29.529	0.898	0.153

Method	Factory						Dining Table					
	Reconstruction			Extrapolation			Reconstruction			Extrapolation		
	PSNR↑	SSIM↑	LPIPS↓	PSNR↑	SSIM↑	LPIPS↓	PSNR↑	SSIM↑	LPIPS↓	PSNR↑	SSIM↑	LPIPS↓
HexPlane	19.109	0.479	0.637	24.266	0.677	0.470	16.687	0.516	0.601	23.127	0.725	0.395
TiNeuVox	<u>24.857</u>	<u>0.705</u>	<u>0.346</u>	22.467	0.747	0.292	<u>21.476</u>	<u>0.658</u>	0.368	20.529	0.768	0.276
DeformGS	21.703	0.621	0.376	23.471	0.787	<u>0.196</u>	15.832	0.488	0.621	21.244	0.784	0.258
Grid4D	21.822	0.631	0.377	22.119	0.765	0.235	16.407	0.475	0.595	19.516	0.741	0.313
NVFi	18.889	0.503	0.655	25.415	0.690	0.496	15.206	0.485	0.681	22.790	0.711	0.428
GSPrediction	17.388	0.588	0.609	21.723	0.713	0.308	13.451	0.546	0.688	18.214	0.679	0.374
TRACE	22.012	0.581	0.426	27.177	0.817	0.234	23.434	0.705	<u>0.380</u>	<u>32.078</u>	0.900	0.169
FreeGave	19.448	0.498	0.485	<u>28.190</u>	<u>0.827</u>	0.221	20.194	0.643	0.433	32.443	0.900	<u>0.159</u>
ParticleGS	31.627	0.912	0.126	32.679	0.943	0.077	20.461	0.636	0.444	31.037	<u>0.886</u>	0.143

Table 7. Full quantitative results on the Dynamic Multipart dataset, rendered at the source resolution. **Bold** and underline indicate the best and second best performance.

Method	Folding Chair						Satellite					
	Reconstruction			Extrapolation			Reconstruction			Extrapolation		
	PSNR↑	SSIM↑	LPIPS↓	PSNR↑	SSIM↑	LPIPS↓	PSNR↑	SSIM↑	LPIPS↓	PSNR↑	SSIM↑	LPIPS↓
DeformGS	41.562	0.994	0.009	18.194	0.847	0.123	35.884	0.988	0.010	29.454	0.980	0.014
FreeGave	39.086	0.994	<u>0.010</u>	26.043	0.951	0.037	<u>37.155</u>	0.991	0.010	<u>34.476</u>	0.989	0.007
TRACE	38.286	<u>0.993</u>	0.011	<u>28.724</u>	<u>0.974</u>	<u>0.023</u>	36.647	<u>0.990</u>	0.010	33.612	<u>0.983</u>	<u>0.009</u>
ParticleGS	41.620	0.994	0.009	31.512	0.977	0.015	38.697	0.991	0.010	34.562	0.981	0.017

Method	Stove						Hyperbolic					
	Reconstruction			Extrapolation			Reconstruction			Extrapolation		
	PSNR↑	SSIM↑	LPIPS↓	PSNR↑	SSIM↑	LPIPS↓	PSNR↑	SSIM↑	LPIPS↓	PSNR↑	SSIM↑	LPIPS↓
DeformGS	40.169	0.988	0.027	30.694	0.953	0.030	36.105	0.983	0.031	33.614	0.987	0.015
FreeGave	35.578	<u>0.989</u>	0.028	32.291	<u>0.989</u>	0.021	32.747	0.985	0.034	41.294	0.995	0.011
TRACE	36.201	0.990	0.028	<u>33.869</u>	<u>0.989</u>	<u>0.016</u>	33.942	0.985	0.036	37.628	<u>0.990</u>	<u>0.012</u>
ParticleGS	<u>39.115</u>	<u>0.989</u>	0.024	40.069	0.991	0.013	<u>34.998</u>	0.984	0.032	<u>38.399</u>	<u>0.990</u>	0.012

Table 8. Full quantitative results on the FreeGave-GoPro dataset, rendered at the source resolution. **Bold** and underline indicate the best and second best performance.

Method	Box						Collision					
	Reconstruction			Extrapolation			Reconstruction			Extrapolation		
	PSNR↑	SSIM↑	LPIPS↓	PSNR↑	SSIM↑	LPIPS↓	PSNR↑	SSIM↑	LPIPS↓	PSNR↑	SSIM↑	LPIPS↓
DeformGS	19.505	0.810	0.221	25.754	0.900	0.139	<u>20.012</u>	<u>0.840</u>	0.209	18.986	0.810	0.251
TRACE	20.203	<u>0.833</u>	0.195	27.987	0.912	<u>0.131</u>	20.242	0.841	0.209	23.447	0.858	0.193
FreeGave	19.800	0.830	<u>0.197</u>	<u>28.661</u>	<u>0.913</u>	<u>0.131</u>	19.608	<u>0.840</u>	0.212	<u>24.188</u>	<u>0.867</u>	<u>0.187</u>
ParticleGS	<u>20.122</u>	<u>0.831</u>	0.195	29.057	0.919	0.102	19.759	0.841	<u>0.211</u>	24.239	0.901	0.157

Method	Wrist Rest						Hammer					
	Reconstruction			Extrapolation			Reconstruction			Extrapolation		
	PSNR↑	SSIM↑	LPIPS↓	PSNR↑	SSIM↑	LPIPS↓	PSNR↑	SSIM↑	LPIPS↓	PSNR↑	SSIM↑	LPIPS↓
DeformGS	19.498	0.829	0.222	19.007	0.808	0.244	20.067	0.835	0.198	23.992	0.896	0.152
TRACE	19.079	<u>0.833</u>	<u>0.209</u>	22.488	0.845	<u>0.204</u>	20.077	0.842	0.195	28.924	0.919	<u>0.137</u>
FreeGave	19.807	0.835	0.208	23.456	0.853	0.197	20.407	<u>0.840</u>	<u>0.194</u>	28.521	<u>0.917</u>	<u>0.137</u>
ParticleGS	<u>19.613</u>	0.835	0.208	<u>23.000</u>	<u>0.846</u>	0.208	20.301	0.842	0.193	<u>28.816</u>	<u>0.917</u>	0.136

Method	Pen1						Pen2					
	Reconstruction			Extrapolation			Reconstruction			Extrapolation		
	PSNR↑	SSIM↑	LPIPS↓	PSNR↑	SSIM↑	LPIPS↓	PSNR↑	SSIM↑	LPIPS↓	PSNR↑	SSIM↑	LPIPS↓
DeformGS	21.180	0.851	0.205	20.577	0.865	0.197	20.372	0.824	0.217	21.674	0.870	0.190
TRACE	20.977	<u>0.854</u>	0.205	26.703	<u>0.917</u>	0.149	<u>20.040</u>	<u>0.829</u>	0.214	25.939	0.899	0.167
FreeGave	20.130	0.853	<u>0.206</u>	<u>27.673</u>	0.923	<u>0.143</u>	19.968	0.830	<u>0.215</u>	<u>26.563</u>	<u>0.903</u>	<u>0.162</u>
ParticleGS	<u>21.079</u>	0.856	0.205	27.746	0.923	0.140	19.824	<u>0.829</u>	<u>0.215</u>	27.879	0.910	0.158